

## Multi-wavelength light absorption of black and brown carbon at a high-altitude site on the Southeastern margin of the Tibetan Plateau, China

Zhuzi Zhao<sup>a,b</sup>, Junji Cao<sup>b,c,\*</sup>, Judith C. Chow<sup>f</sup>, John G. Watson<sup>f</sup>, Antony L-W. Chen<sup>e</sup>, Xiaoliang Wang<sup>f</sup>, Qiyuan Wang<sup>b</sup>, Jie Tian<sup>b</sup>, Zhenxing Shen<sup>d</sup>, Chongshu Zhu<sup>b</sup>, Suixin Liu<sup>b</sup>, Jun Tao<sup>g</sup>, Zhaolian Ye<sup>a</sup>, Ting Zhang<sup>b</sup>, Jiamao Zhou<sup>b</sup>, Ruixia Tian<sup>b</sup>

<sup>a</sup> School of Chemical and Environmental Engineering, Jiangsu University of Technology, Changzhou, Jiangsu, China

<sup>b</sup> Key Laboratory of Aerosol Chemistry and Physics, Institute of Earth Environment, Chinese Academy of Sciences, Xi'an, Shaanxi, China

<sup>c</sup> Institute of Global Environment Change, Xi'an Jiaotong University, Xi'an, Shaanxi, China

<sup>d</sup> Department of Environmental Science and Engineering, Xi'an Jiaotong University, Xi'an, Shaanxi, China

<sup>e</sup> Department of Environmental and Occupational Health, University of Nevada, Las Vegas, NV, USA

<sup>f</sup> Division of Atmospheric Sciences, Desert Research Institute, Reno, NV, USA

<sup>g</sup> South China Institute of Environmental Sciences, Ministry of Environmental Protection, Guangzhou, China

### ARTICLE INFO

#### Keywords:

Aerosol light absorption  
Dust  
Black carbon  
brown carbon  
Climate  
Tibetan plateau

### ABSTRACT

The Tibetan Plateau (TP) is one of the world's most sensitive areas for climate change, but the lack of information on light-absorption by aerosols limits the understanding of climate forcing feedbacks. Here, the contributions of black carbon (BC) and brown carbon (BrC) to light absorption and radiative forcing were investigated. Absorption Ångström exponents ( $\alpha$ ), mass absorption cross sections (MAC), and absorption coefficients ( $b_{\text{abs}}$ ) for selected wavelengths were measured for a year of aerosol samples collected at Lulang on the southeast TP. Aerosol absorption at all wavelengths was strongest in the pre-monsoon when levoglucosan, a biomass burning indicator, was elevated. The contributions of BC, BrC, and dust to  $b_{\text{abs}}$  were decoupled. Results showed that dust contributed 8.5% to the total light absorption at 405 nm and 3.9% at 808 nm. A two-component model indicated that BC and BrC contributed 48.7% and 44.0% to total  $b_{\text{abs}}$  at 405 nm but BrC had a smaller effect at middle-visible wavelengths. Elevated  $b_{\text{abs,non-dust,BC}}$  and  $b_{\text{abs,non-dust,BrC}}$  and a high  $\alpha_{\text{BrC}}$  but low  $\alpha_{\text{aerosol}}$  values in the pre-monsoon were attributed to biomass burning, which produces not only BrC but also BC which has a much lower  $\alpha$  value. Average non-dust MACs for BC and BrC at 405 nm were  $6.1 \pm 2.8$  and  $0.72 \pm 0.55 \text{ m}^2 \text{ g}^{-1}$ , respectively. Nonparametric statistical tests showed that the  $\text{MAC}_{\text{non-dust,BC}}$  was relatively constant but  $\text{MAC}_{\text{non-dust,BrC}}$  was more variable. In addition, BrC was correlated with non-dust  $b_{\text{abs,BC}}$  and  $\text{MAC}_{\text{non-dust,BC}}$  in winter and the pre-monsoon, implying BrC and BC shared sources in those two seasons, but lower correlations in the monsoon and post-monsoon suggest that a mixture of sources impacted BrC (e.g., biogenic emission, secondary formation, etc.). Finally, the relative contributions of BrC to BC for radiative forcing from 405 to 808 nm were  $29.4 \pm 9.5\%$  with no remarkable seasonal differences, confirming the importance of BrC to light absorption in the near UV throughout the year. As a result, the BrC absorption is an important additional factor which needs to be considered in atmospheric models, although the atmospheric heating by BC seems to be a larger climate forcer in this region.

### 1. Introduction

Light absorbing aerosols, mainly black carbon (BC), brown carbon (BrC), and mineral dust (Moosmüller et al., 2009), can contribute to solar radiative forcing by heating layers of the atmosphere that have high aerosol loadings. Often, the dominant light-absorbing aerosol is BC emitted from the incomplete combustion of fossil fuel, biomass, or

biofuels; this type of primary aerosol consists of refractory, water-insoluble, aggregates of carbon spherules (Bond et al., 2013). In contrast, BrC is a fraction of organic carbon (OC) that can share primary sources with BC but also can originate from soil humic matter or biogenic sources (e.g., plant debris and fungi) (Wu et al., 2016). Furthermore, BrC also can form secondarily through chemical reactions involving anthropogenic or biogenic precursors (Laskin et al., 2015). Mineral dust

\* Corresponding author. Key Laboratory of Aerosol Chemistry and Physics, Institute of Earth Environment, Chinese Academy of Sciences, Xi'an, Shaanxi, China.  
E-mail address: [cao@loess.llqg.ac.cn](mailto:cao@loess.llqg.ac.cn) (J. Cao).

<https://doi.org/10.1016/j.atmosenv.2019.05.035>

Received 23 November 2018; Received in revised form 15 May 2019; Accepted 17 May 2019

Available online 18 May 2019

1352-2310/ © 2019 Elsevier Ltd. All rights reserved.

is a term used to indicate airborne mineral particles that can originate from natural sources, such as deserts, or anthropogenic sources including construction and industrial activities (Moosmüller et al., 2009).

The spectral dependence of aerosol light absorption is commonly described by a power law relationship and parameterized as  $\lambda^{-\alpha}$ , where  $\lambda$  refers to the wavelength (nm) and  $\alpha$  is the aerosol absorption Ångström exponent. BC absorbs solar radiation over a broad spectral range, from the ultraviolet (UV) to infrared (IR), with  $\alpha$  values close to unity (Bond et al., 2013). In comparison with BC, BrC absorbs light with a stronger wavelength-dependence with  $\alpha > 1$  (Andreae and Gelencsér, 2006; Laskin et al., 2015). The light absorption by mineral aerosol particles varies with their mineralogical composition (Caponi et al., 2017; Moosmüller et al., 2009; Yang et al., 2009). Previous studies have shown that BC is important for climate, and its radiative effects typically lead to warming at the top of the atmosphere but cooling at the Earth's surface (Ramanathan et al., 2007; Rengarajan et al., 2007). More recently, light absorbing organic substances have attracted widespread attention owing to their potential climate forcing effects over regional, continental, and even global scales (Bahadur et al., 2012; Feng et al., 2013; Jo et al., 2016; Lin et al., 2014). In this regard, Lin et al. (2014) estimated that the global light absorption caused by BrC was  $0.22 \text{ W m}^{-2}$  to  $0.57 \text{ W m}^{-2}$ , equivalent to 27%–70% of the BC absorption. Using atmospheric abundances of BrC based on global simulations, Feng et al. (2013) showed that radiative forcing changes from  $-0.08 \text{ W m}^{-2}$  to  $+0.025 \text{ W m}^{-2}$  by organic aerosols at the top of the atmosphere.

The Tibetan Plateau (TP), the world's largest and highest plateau, is a sensitive area for climate change and vulnerable to impacts from anthropogenic activities. Light-absorbing aerosols can reduce the snow albedo, decrease upwelling radiation, and thereby contribute to glacial retreat processes (Gertler et al., 2016; Li et al., 2017; Yang et al., 2015). Previous studies have shown that the transport of polluted air from south Asia to the high Himalayas has impacted the Tibetan environment (Bonasoni et al., 2010; Li et al., 2016b; Marcq et al., 2010; Zhao et al., 2013, 2017). Besides pollutants transported over long distances, local emissions from residential burning activities and fossil fuel combustion also played an important role in atmospheric pollution as well as glaciers retreats in TP (Li et al., 2018). To date, the light absorption of aerosols in the Himalayas and TP has focused on BC and dust particles, and there is little information regarding the role of light-absorbing organic species (Kirillova et al., 2016). Because of their potential significance for the Earth's radiative balance, the lack of ground-based observations and poor characterization of organic aerosols limits our ability to assess climate forcing feedbacks in general and for the TP specifically (Kirillova et al., 2014a, 2014b, 2016; Srinivas and Sarin, 2014).

Numerous studies have investigated the optical properties of BrC in the atmosphere using filter-based solvent extraction methods or online/offline optical measurements of the extinction and/or absorption coefficients of aerosol particles. Chemical and optical methods can both be used to measure light-absorbing aerosols with emphasis on different aspects of their properties, hence cannot be totally substituted by one another (Ran et al., 2016). Typical optical instruments include aethalometers (Hansen et al., 1984), multi-angle absorption photometer (MAAP) (Petzold et al., 2005), particle soot absorption photometer (PSAP) (Virkkula et al., 2005) and, most recently, multi-wavelength absorbance analyzer (MWAA) (Massabò et al., 2015) and multi-wavelength thermal/optical carbon analyzers (Chen et al., 2015; Chow et al., 2015), which measuring the transmission of light through particle-loaded filters to quantify aerosol optical properties. And chemical methods focus on the light absorption caused by extracted materials such as humic-like substances (HULIS), water-soluble OC, and methanol-soluble OC. However, due to the sample treatments before analysis, some information of aerosol absorption properties might be lost or modified.

Indeed, it is challenging to disentangle the BrC contribution to

direct radiative forcing from that of BC and dust particles (Kirillova et al., 2016). For many light absorption studies, light absorption by BC and BrC can be differentiated by the absorption Ångström exponent (AAE) values, assuming that the AAE = 1 for BC (sometimes also termed elemental carbon or EC) to derive the BrC absorption (Chow et al., 2018; Healy et al., 2017). Recently researches carried on the TP (Hu et al., 2017; Kirillova et al., 2016; Li et al., 2016b; Wu et al., 2019) mostly focus on light absorption of solvent extracted fractions. Zhu et al. (2017) studied the spectral dependence of aerosol absorption using a multi-wavelength Aethalometer™ deployed at various sites on the TP, which revealed the relatively high percentage of BrC absorption contribution in the remote area. Nonetheless, the current understanding of the spectral aerosol absorptive properties over the TP is still quite limited, especially the temporal variability that can only be understood through long-term monitoring.

To investigate the seasonal variations in aerosol light absorption, a full year of samples (July 16, 2008 to July 26, 2009) was collected at Lulang, a high-altitude site on the southeast TP, China. In total, 61 total suspended particle (TSP) samples were analyzed by multi-wavelength thermal-optical techniques to characterize absorption coefficients ( $b_{\text{abs}}$ ) for wavelengths from 405 to 808 nm (Chen et al., 2015; Chow et al., 2015). After accounting for the impacts of dust, a simplified two-component model was used to quantify the BC and BrC contributions to light absorption. The main objectives of this study were to: (1) characterize separately the contributions of BC and BrC to light absorption; (2) estimate the mass absorption cross sections (MACs) of BC and BrC and evaluate the MAC seasonal variations; and (3) assess the relative contributions of BC and BrC to radiative forcing.

## 2. Materials and methods

### 2.1. Sampling

The Lulang sampling site used for our studies (94.44°E, 29.46°N, altitude 3300 m) is situated in Linzhi Prefecture on the southeastern margin of the TP. The Yarlung Tsangpo River Valley lies to the west, and the Himalaya Mountains rise to the south. There are extensive forests in Linzhi prefecture, and the sampling site is located in a remote area with no major anthropogenic sources nearby. However, Lulang is approximately 30–50 km west of several small villages (Cao et al., 2010). Hence, emissions from domestic biomass burning for cooking and heating, as well as long-range transport to the Plateau from upwind regions (e.g., South and Southeast Asia) (Gustafsson et al., 2009) are possible sources of pollutants.

To achieve adequate loadings for chemical analysis, sampling was conducted once every sixth day starting at 10:30 Beijing Time for 72 h from July 16, 2008 to July 26, 2009. TSP samples were collected on 90 mm quartz-fiber filters (QM-A™, Whatman, Clifton, NJ, USA) with a KC-120H sampler (Laoshan Electronic Instrument Factory Co., LTD., QingDao, China). The flow rate of the sampler was reduced from  $100 \text{ L min}^{-1}$  to  $40 \text{ L min}^{-1}$  to adjust for the low atmospheric surface pressure at the high-altitude site ( $\sim 681.4 \pm 2.6 \text{ hpa}$ ). Prior to sampling, the filters were pre-combusted at  $900 \text{ }^\circ\text{C}$  for 3 h to remove any residual carbon. Field blanks were collected every season by exposing filters in the sampler without activating the pump; these were used to account for potential contamination introduced during the sample transport and handling processes. After sampling, the filters stored in airtight containers and shipped to the Institute of Earth Environment in Xi'an. The samples were stored in refrigerator at  $-18 \text{ }^\circ\text{C}$  to avoid the loss of volatile compounds before and after analysis.

Based on a discussion of the meteorological characteristics of Lulang in Zhao et al. (2017), the data obtained for the site was divided into four seasons. These are (1) the pre-monsoon (18 February 2009 to 27 April 2009), (2) the monsoon (16 July 2008 to 3 October 2008; 28 April 2009 to 26 August 2009), (3) the post-monsoon (4 October 2008 to 9 November 2008), and (4) winter (10 November 2008 to 17 February

2009).

## 2.2. Laboratory analyses

### 2.2.1. Measurement of the light-absorbing properties

**2.2.1.1. Attenuation ( $ATN_{\lambda}$ ).** The optical properties of the filter samples were measured with a DRI Model 2015 multiwavelength thermal/optical carbon analyzer (Magee Scientific, Berkeley, CA, USA) following the IMPROVE\_A protocol (Chow et al., 2007). The analyzer used sequentially-modulated diode lasers to quantify the light attenuation of the particle-laden filter at seven wavelengths (405, 445, 532, 635, 780, 808 and 980 nm) as well as OC, EC concentrations in 0.526 cm<sup>2</sup> punches of the quartz-fiber filters. A detailed description of the analyzer is given in Chow et al. (2015). Fig. S1 shows that some samples retained a reddish tinge after carbon analyses which is an indication of mineral deposits.

Particle light absorption by particles was estimated by transmittance attenuation (ATN):

$$ATN_{\lambda} = -\ln\left(\frac{FT_{\lambda, i}}{FT_{\lambda, f}}\right) \quad (1)$$

where  $\lambda$  is the measurement wavelength,  $FT_{\lambda, i}$  and  $FT_{\lambda, f}$  are the filter transmittances at wavelength  $\lambda$  at the beginning and end of thermal analysis, respectively.  $FT_{\lambda, f}$  approximates a blank filter because all of the carbon has been removed at the end of the analysis. Results for 532 nm and 980 nm are not shown owing to low signal-to-noise ratios.

Filter-based absorption methods can be affected by measurement artifacts associated with the filter substrate, aerosol scattering, and particle loading, etc. (Chow et al., 2018; Coen et al., 2010; Jimenez et al., 2007). Therefore, it is necessary to compensate for any artifacts that cause deviations from Beer's law (Arnott et al., 2005; Virkkula et al., 2005) as described below.

**2.2.1.2. Light absorption coefficient ( $b_{abs, \lambda}$ ).** To account for filter matrix artifacts, the  $ATN_{\lambda}$  values were corrected for particle light absorption optical depth ( $ABS_{\lambda}$ ) using regression equations established by Chen et al. (2015). Briefly, Chen considered EC2 step (740 °C in a 98% He/2% O<sub>2</sub> atmosphere) based on IMPROVE\_A analysis is exclusively EC for diesel soot samples with negligible BrC and POC. Then,  $ATN_{\lambda}$  from all 1 s measurements at EC2 step for diesel exhaust samples were retrieved. Meanwhile, the multi-wavelength  $ABS_{\lambda}$  was calculated from a MAE of 7.4 m<sup>2</sup> g<sup>-1</sup> multiply by the temporal variation in [EC] at each second throughout EC2 step. Finally, the instrument-specific relationships between ATN and ABS by each wavelength as followed:

$$ABS_{\lambda} = a_{\lambda} \times ATN^2 + b_{\lambda} \times ATN \quad (2)$$

Where  $a_{\lambda}$  and  $b_{\lambda}$  are coefficients that include wavelength-specific multiple scattering and loading effects. These ABS–ATN relationships would apply to any samples, regardless of the nature of light-absorbing material (Chen et al., 2015).

Finally, the light absorption coefficient ( $b_{abs}$ ) at each wavelength  $\lambda$  can be calculated as follows:

$$b_{abs, \lambda} = \frac{ABS_{\lambda} \times A}{V} \quad (3)$$

where A and V indicate the filter's area (cm<sup>2</sup>) and sampling volume (m<sup>3</sup>), respectively. More detailed descriptions of the procedures and empirical formulas used are provided in Chen et al. (2015).

### 2.2.2. Analysis of the chemical components

**2.2.2.1. Carbonaceous material.** The filter mass loadings of OC and elemental carbon (EC) (in units of  $\mu\text{g cm}^{-2}$ ) were quantified using a single wavelength DRI\_2001A OCEC analyzer (Atmoslytic Inc., Calabasas, CA, USA) following the IMPROVE\_A protocol (Chow et al., 2004). Specific quality assurance/quality control (QC/QA) procedures

for carbon analyses have been described in Chow et al. (2011). Data about OC and EC have been reported by our previous work (Zhao et al., 2013). Relatively good correlations in OC, EC and TC between DRI\_2001A and DRI\_2015 analyzer (slope: 0.88 to 1.09,  $r^2 = 0.85$  to 0.93, Fig. S2 in supplement), indicating that the samples have been well preserved, and the data set were reliable. To keep consistency with the previous work, data cited here to estimate MAC of BC and BrC.

**2.2.2.2. Levoglucosan.** Three 0.526 cm<sup>2</sup> punches of each sample were composited, extracted with 10 mL deionized water for 30 min with ultrasonication, and then filtered through a 0.45  $\mu\text{m}$  pore size microporous membrane to remove insoluble material. Levoglucosan, a specific biomarker only generated from biomass burning (Simoneit et al., 1999), was measured using high-performance anion-exchange chromatography (HPAEC) with pulsed amperometric detection (PAD) (Watson et al., 2017). The HPAEC-PAD system consisted of a Dionex ICS-3000 series ion chromatograph (Dionex Corp., Sunnyvale, CA, USA) with a quaternary pump and degasser, a column compartment, an electrochemical detector and a gold electrode. The minimum detection limit for levoglucosan was 0.002 mg L<sup>-1</sup> or 0.064  $\mu\text{g m}^{-3}$ . More details for this analyses may be found in Shen et al. (2017).

**2.2.2.3. Elemental iron.** The concentrations of elemental iron (Fe) on the quartz-fiber filters, an indicator of mineral dust were determined using an energy dispersive X-ray fluorescence (ED-XRF) spectrometer (Epsilon 5 XRF analyzer, PANalytical, Almelo, the Netherlands). It is better using Teflon-membrane to detect elements concentration by ED-XRF. However, we didn't use the Teflon filter to collect samples at lulang due to limited resources. For QAQC of iron measurements by ED-XRF, NIST Standard Reference Material (SRM) 2783 was employed to validate the accuracy of the instrument. The relative errors for all measured elements were well within the required range of error ( $\leq 6\%$  between SRM 2783 and ED-XRF results), demonstrating the accuracy of our ED-XRF. Replicate analysis of quartz-fiber sample, cross check by co-located Teflon-membrane filters were also carried out. XRF measurements on 30 collocated Teflon-membrane and quartz-fiber filters from Xi'an were comparable with correlation ( $r^2$ ) at 0.95 for Fe (with slopes of 0.96). Replicate analysis of one quartz-filter sample (five times) yielded an analytical precision below 10%. The MDLs was 0.015  $\mu\text{g cm}^{-2}$  for Fe in quartz-fiber sample. Details of the ED-XRF measurements are described in the previous publication (Xu et al., 2016).

## 3. Calculations

### 3.1. Segregation of black carbon, brown carbon and dust

The total bulk absorption coefficient ( $b_{abs, \lambda}$ ) was first separated into the dust ( $b_{abs, dust, \lambda}$ ) and non-dust ( $b_{abs, non-dust, \lambda}$ ) absorption components as follows:

$$b_{abs, non-dust, \lambda} = b_{abs, \lambda} - b_{abs, dust, \lambda} \quad (4)$$

where

$$b_{abs, dust, \lambda} = [C_{dust}] \times MAC_{dust, \lambda} \quad (5)$$

For Equation (5), the  $MAC_{dust, \lambda}$  values were taken from a study by Caponi et al. (2017) in which 12 mineral dust samples were collected from different sources worldwide, the absorption coefficients were determined, and the UV to NIR light-absorbing properties ( $\alpha$  and MAC) were evaluated. Using the data for raw soils collected in the Gobi desert by Caponi et al. (2017), the  $MAC_{dust}$  values were calculated to match the Model\_2015 OCEC analyzer wavelengths: 0.056, 0.042, 0.014, 0.007 and 0.006 m<sup>2</sup> g<sup>-1</sup> at 405, 445, 635, 780 and 808 nm, respectively. The dust concentrations ( $C_{dust}$ ) were estimated by dividing the measured elemental Fe concentrations by 4.79%; this conversion was based on a prior study which showed that Fe accounts for 4.79% of the

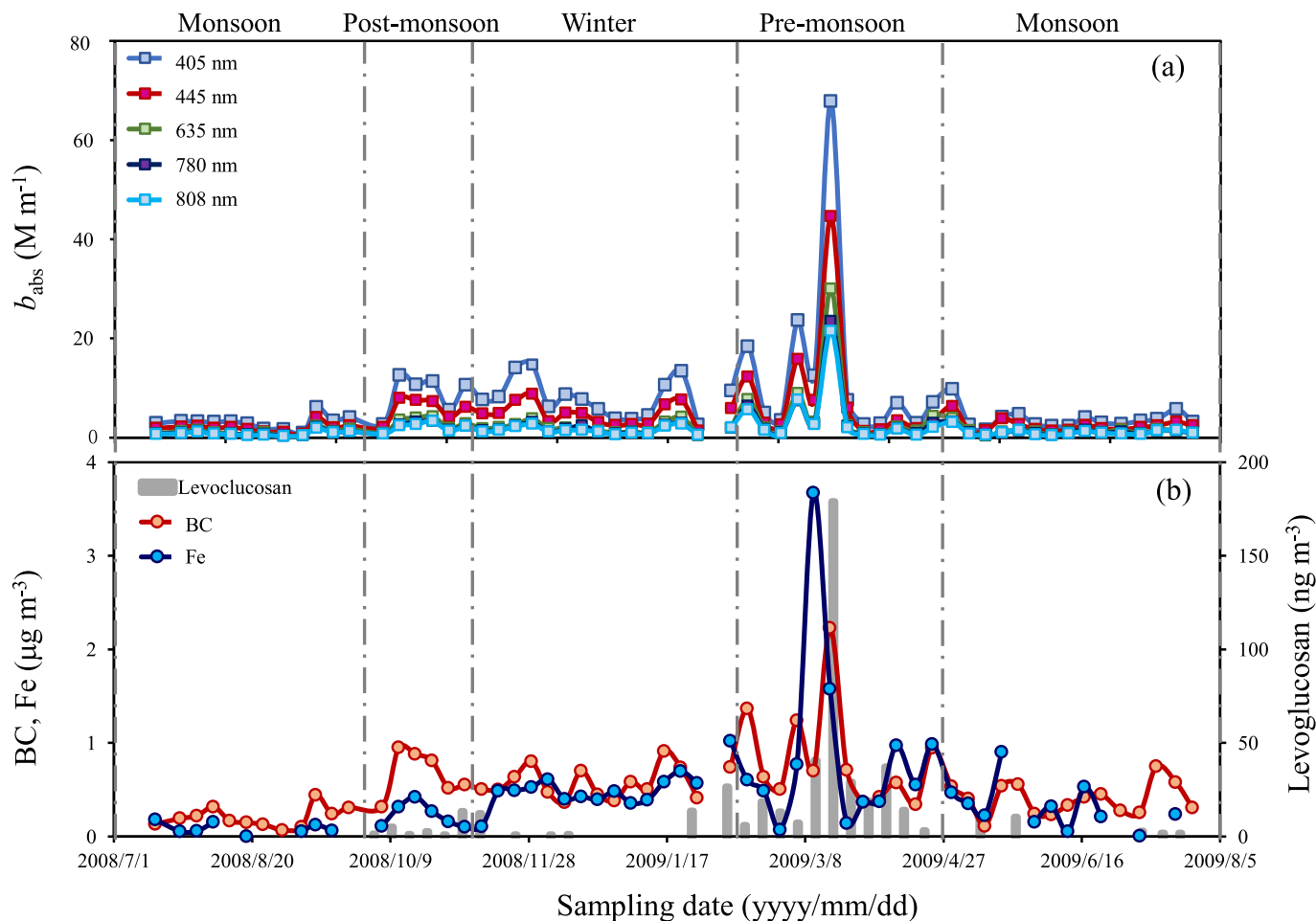


Fig. 1. Temporal variations of (a) aerosol light absorption coefficients ( $b_{\text{abs}}$ ,  $\text{M m}^{-1}$ ) measured at wavelengths of 405, 445, 635, 780, and 808 nm, (b) black carbon and iron (BC and Fe, respectively,  $\mu\text{g m}^{-3}$ ) and levoglucosan ( $\text{ng m}^{-3}$ ) concentrations from July 16, 2008 to July 26, 2009.

TP top soil (Li et al., 2009).

A simplified two-component model (Chen et al., 2015) was used to separate BC and BrC for the non-dust light absorption:

$$b_{\text{abs, non-dust}, \lambda} = b_{\text{abs, non-dust}, \text{BC}, \lambda} + b_{\text{abs, non-dust}, \text{BrC}, \lambda} \\ = q_{\text{BC}} \times \lambda^{-\alpha_{\text{BC}}} + q_{\text{BrC}} \times \lambda^{-\alpha_{\text{BrC}}} \quad (6)$$

where  $q_{\text{BC}}$  and  $q_{\text{BrC}}$  are fitting coefficients, and the absorption Ångström exponents for BC and BrC ( $\alpha_{\text{BC}}$  and  $\alpha_{\text{BrC}}$ , respectively) explain the spectral dependence of  $b_{\text{abs, non-dust}, \lambda}$ . This approach is analogous to that used by Bernardoni et al. (2017) and Massabò et al. (2015) who quantified BrC light absorption contributions from BC. Assuming  $\alpha_{\text{BC}} = 1$  (Andreae and Gelencsér, 2006) and constraining  $\alpha_{\text{BrC}}$  within its possible range (1.5–15) (Eklund et al., 2014), the fitting coefficients (i.e.,  $q_{\text{BC}}$  and  $q_{\text{BrC}}$ ) are determined by least squares minimization between the measured and calculated values. The overall best fit corresponding to the low mean squared error is selected as the effective  $\alpha_{\text{BrC}}$  (Chow et al., 2018).

### 3.2. Experimental Absorption Ångström exponents ( $\alpha$ ) for non-dust aerosol

Absorption Ångström exponents were calculated as a function of wavelength using a power law equation:

$$b_{\text{abs, non-dust}, \lambda} = k_1 \times \lambda^{-\alpha_{\text{aerosol}}} \quad (7)$$

where  $k_1$  and  $k_2$  is a fitting constant and the aerosol is defined as  $\text{BrC} + \text{BC}$ ; similarly, the non-dust  $\alpha$  for BrC can be calculated as:

$$b_{\text{abs non-dust}, \text{BrC}, \lambda} = k_2 \times \lambda^{-\alpha_{\text{BrC}}} \quad (8)$$

### 3.3. Mass absorption cross sections (MAC) of non-dust BC and BrC

According to Olson et al. (2015), the non-dust BC MAC for a given wavelength ( $\text{MAC}_{\text{non-dust}, \text{BC}, \lambda}$ ) can be calculated by dividing the  $b_{\text{abs, non-dust}, \text{BC}, \lambda}$  by the BC concentration; and similarly the BrC MAC ( $\text{MAC}_{\text{non-dust}, \text{BrC}, \lambda}$ ) can be calculated by dividing  $b_{\text{abs, non-dust}, \text{BrC}, \lambda}$  by the OC concentration. As BrC is only a fraction of OC, the derived  $\text{MAC}_{\text{non-dust}, \text{BrC}}$  should be regarded as a lower limit of the actual  $\text{MAC}_{\text{BrC}}$ .

### 3.4. Radiative forcing

The relative radiative forcing of BrC to BC across the solar absorption wavelength has been assessed by Kirillova et al. (2014b). Briefly, the fractional solar absorption of BrC in our study was obtained by multiplying the wavelength-dependent solar emission flux ( $I_0(\lambda)$ ) (Levinson et al. (2010) by the BrC light absorption (integrated for wavelengths between 405 and 808 nm) which was normalized to BC. Briefly, the light absorption of BrC [ $\frac{I_0 - I}{I_0}(\lambda, \text{BrC})$ ] and BC [ $\frac{I_0 - I}{I_0}(\lambda, \text{BC})$ ] were calculated using the Beer-Lambert law (Kirillova et al., 2014a):

$$\frac{I_0 - I}{I_0}(\lambda, \text{BrC}) = 1 - e^{-\left(\text{MAC}_{\text{BrC}} \left[\frac{\lambda_0}{\lambda}\right]^{\alpha_{\text{BrC}}} C_{\text{OC}} \cdot \text{BLH}\right)} \quad (9)$$

$$\frac{I_0 - I}{I_0}(\lambda, \text{BC}) = 1 - e^{-\left(\text{MAC}_{\text{BC}} \left[\frac{\lambda_0}{\lambda}\right]^{\alpha_{\text{BC}}} C_{\text{BC}} \cdot \text{BLH}\right)} \quad (10)$$

where  $MAC_{BrC}$  and  $MAC_{BC}$  are the mass absorption cross sections for non-dust BrC and BC,  $\alpha_{BrC}$  was the absorption Ångström exponents calculated within 405–808 nm, and  $\alpha_{BC}$  was set as 1, respectively. The reference wavelength ( $\lambda_0$ ) was 405 nm, and  $\lambda$  refers to the wavelengths of 405, 445, 635, 780 and 808 nm. Likewise,  $C_{OC}$ ,  $C_{BC}$  and BLH correspond to the mass concentrations of OC, BC (in  $\mu\text{g m}^{-3}$ ) and atmospheric boundary layer height, respectively. The BLHs at 3-h intervals from UTC 0:00–23:00 for the station were obtained from European Centre for Medium-range Weather Forecasts (ECMWF). The BLH data at UTC 03:00 and 06:00 (the deep boundary-layer dynamics in a day) were chosen and integrated over the periods corresponding to the sample duration.

Finally, the fractional contribution of solar absorption by BrC relative to BC was calculated as follows:

$$f = \frac{\int_{405}^{808} I_0(\lambda) \left[ \frac{I_0 - I}{I_0}(\lambda, \text{BrC}) \right] d\lambda}{\int_{405}^{808} I_0(\lambda) \left[ \frac{I_0 - I}{I_0}(\lambda, \text{BC}) \right] d\lambda} \quad (11)$$

## 4. Results and discussion

### 4.1. Characteristics of the absorption coefficient ( $b_{abs, \lambda}$ )

The annual averages (arithmetic means  $\pm$  standard deviations) for  $b_{abs, \lambda}$  were  $7.1 \pm 9.2$ ,  $4.5 \pm 6.0$ ,  $2.4 \pm 3.7$ ,  $2.0 \pm 2.9$  and  $1.8 \pm 2.8 \text{ Mm}^{-1}$  at  $\lambda = 405, 445, 635, 780$  and  $808$  nm, respectively. The 72-h averaged ratio of  $b_{abs, 405}/b_{abs, 808}$  varied from 2.6 to 6.2, with a grand average of 4.1, indicating impacts from non-BC light absorption at short wavelengths. As shown in Fig. 1a, large temporal and seasonal variations were found for  $b_{abs}$ , ranged from 0.9 to  $67.8 \text{ Mm}^{-1}$  at 405 nm and from 0.3 to  $20.6 \text{ Mm}^{-1}$  at 808 nm. The highest  $b_{abs}$  were found in the pre-monsoon season, followed by the post-monsoon and winter. Table 1 shows that the seasonal averaged  $b_{abs, 405}$  varied from  $3.4 \pm 1.7 \text{ Mm}^{-1}$  during the monsoon to  $8.1 \pm 3.8 \text{ Mm}^{-1}$  during winter and  $13.4 \pm 18.4 \text{ Mm}^{-1}$  during the pre-monsoon. Similar patterns were found for  $b_{abs, 808}$  but with 70%–80% lower values, with ranging from  $0.97 \pm 0.6 \text{ Mm}^{-1}$  in the monsoon to  $3.9 \pm 5.7 \text{ Mm}^{-1}$  during the pre-monsoon.

As discussed by Zhao et al. (2017), regional meteorology, boundary-layer dynamics, and biomass burning emissions can lead to enhanced pollution transport from sub-Himalayan and south Asia regions to the sampling site during the pre-monsoon season, and this can result in high  $b_{abs}$ . In contrast, the low  $b_{abs}$  values during the monsoon season can be explained by the intense precipitation (Zhao et al., 2013). Relatively low wintertime  $b_{abs}$  ( $1.53 \text{ Mm}^{-1}$  at 808 nm to  $8.07 \text{ Mm}^{-1}$  at 405 nm) can be attributed to low mixing layer heights (Zhao et al., 2017) that tend to inhibit pollution transport.

Time series plots of BC, Fe and levoglucosan concentrations are shown in Fig. 1(b). Good correlations were found between  $b_{abs}$  and BC at different wavelengths (with a correlation coefficient,  $r^2 = 0.72$  to  $0.77$ , at  $p < 0.001$ ), reinforcing idea that BC was the dominant aerosol component affecting  $b_{abs}$ . Levoglucosan was more abundant during late winter and the pre-monsoon, indicating the biomass burning is a major emission source in these periods. However, major peaks in levoglucosan and Fe found in the pre-monsoon season did not always coincide with BC and  $b_{abs}$ , suggesting impacts from multiple sources (residential wood combustion, secondary organic carbon formation, aged aerosols, biogenic aerosols, etc.) to  $b_{abs}$ . One would expect that high Fe loadings would be related to wind speed and transport. In addition, it worth noting that in an episode event (March 11th to Marth 17th, 2009) strongly impacted of long-range transport of pollutants from upwind sources (including eastern India and Bangladesh) has been proved by previous studies (Lüthi et al., 2015; Xia et al., 2011; Zhao et al., 2013), BC increased by three to four folds while  $b_{abs}$  increased by eight to nine times. As BrC, BC, and dust tend to mix with one another during

transport and aging (Lack and Cappa, 2010; Liu et al., 2015), radiative forcing can increase due to a lensing effect (Wu et al., 2016). Thus, the optical properties of the aerosol almost certainly changed as the particles aged during long-range transport.

### 4.2. Light absorption by dust, BC, and BrC

We evaluated the contribution of mineral dust ( $b_{abs, dust}$ ) to particle light absorption before evaluating the separate contributions of BC and BrC based on the Eq. (6). Table 1 shows that the contribution of  $b_{abs, dust}$  to total  $b_{abs, measured}$  at 405 nm was relatively high (12.6%) during pre-monsoon, which is when the surface wind speeds were the highest of the year, up to 1.93 m/s. For comparison, the percent contributions of dust to absorption for the other seasons were 7.0% for the monsoon, 3.4% for the post-monsoon, and 9.0% for winter. The annual average values for the  $b_{abs, dust}$  to total  $b_{abs, measured}$  ratios were 8.5% at 405 nm, 7.4% at 635 nm and 3.9% at 808 nm.

Fig. 2(a) illustrates the contributions of dust, BC and Br to the total  $b_{abs}$  ( $b_{abs, measured}$ ) at 405 nm. The annual average  $b_{abs, non-dust, BrC, 405}$  was  $3.2 \pm 3.6 \text{ Mm}^{-1}$  (range: 0.14 to  $24.1 \text{ Mm}^{-1}$ ) and the  $b_{abs, non-dust, BC, 405}$  was  $3.5 \pm 5.6 \text{ Mm}^{-1}$  (range: 0.6 to  $41.8 \text{ Mm}^{-1}$ ); thus BrC and BC accounted for relatively similar percentages of total  $b_{abs, measured}$ , 44.0% and 48.7% respectively. The sizeable contribution of light absorption attributable to BrC for the UV and short visible wavelengths indicates that this material is important for radiative forcing and photochemistry. In terms of seasonal variations, both  $b_{abs, non-dust, BrC, 405}$  and  $b_{abs, non-dust, BC, 405}$  showed stronger in the pre-monsoon compared with other seasons. For example,  $b_{abs, non-dust, BC, 405}$  values were  $7.5 \pm 11.6$ ,  $1.9 \pm 1.1$ ,  $4.3 \pm 1.9$  and  $2.9 \pm 1.5$  while  $b_{abs, non-dust, BrC, 405}$  were  $4.8 \pm 6.5$ ,  $1.4 \pm 0.8$ ,  $4.4 \pm 2.2$  and  $4.6 \pm 2.4 \text{ Mm}^{-1}$  in the pre-monsoon, monsoon, post-monsoon, and winter, respectively. Recently study on source emission characteristics of BrC by combustion chamber experiments reported that BrC from biomass burning contributed to 41–85% of the total particles light absorption at 370 nm, while that from coal burning was much lower, which only accounted for 15–18% (Tian et al., 2019). The contribution of  $b_{abs, non-dust, BrC, 405}$  to total absorption were 37.0% in pre-monsoon, 39.8% in monsoon, 48.4% in post-monsoon and 55.2% in winter, which are close to the values for crop residues, indicating possible impacts of biomass burning emissions to  $b_{abs}$  throughout the sampling time. The lowest  $b_{abs, non-dust, BrC, 405}/b_{abs, non-dust, 405}$  ratio in pre-monsoon is consistent with elevated  $b_{abs, non-dust, BC}$ , which might be due to a combination of high BC concentrations and internal mixing, the latter of which could result from the formation of coatings or aging during long range transport (Zhao et al., 2017).

Fig. 2(b) shows time series plots of the MAC values for non-dust BC and non-dust BrC at 405 nm. The annual average  $MAC_{non-dust, BC, 405}$  was  $6.1 \pm 2.8 \text{ m}^2 \text{ g}^{-1}$ , and the seasonal values were comparable for the monsoon ( $6.6 \pm 2.4 \text{ m}^2 \text{ g}^{-1}$ ), pre-monsoon ( $6.4 \pm 4.6 \text{ m}^2 \text{ g}^{-1}$ ), and post-monsoon ( $6.2 \pm 1.6 \text{ m}^2 \text{ g}^{-1}$ ), but lower in winter ( $4.9 \pm 1.8 \text{ m}^2 \text{ g}^{-1}$ ). It should be noted that the  $MAC_{non-dust, BC, 405}$  (or any wavelengths) is lower than the values (e.g. at least  $5 \text{ m}^2/\text{g}$  at 550 nm) reported in previous work (Bond et al., 2013). The phenomenon was also found in Chen et al. (2015) in wildfire samples, which could be explained by a continuum of light-absorbing carbon from biomass burning – ranging from BrC and Char to soot (Masiello, 2004; Pöschl, 2003). As char and soot resulting from pyrolysis and high-temperature graphitization, respectively, are both quantified as EC (Han et al., 2009), they may have distinct optical properties.  $b_{abs}$  that was calibrated against diesel EC would represent just the soot fraction because there is little char material in diesel exhaust. It is possible that our samples have more char than soot, and therefore have a lower MAC. The highest  $MAC_{non-dust, BC, 405}$  value ( $18.7 \text{ m}^2 \text{ g}^{-1}$ ) was found on 17 March 2009, which was in the pre-monsoon, and that coincided with high  $b_{abs, non-dust, BC, 405}$  ( $41.8 \text{ Mm}^{-1}$ ) as well as high loadings of BC ( $2.23 \mu\text{g m}^{-3}$ ) and levoglucosan ( $178.9 \text{ ng m}^{-3}$ ). Nonparametric

**Table 1**Aerosol light absorption coefficients ( $b_{\text{abs}}$ , Mm<sup>-1</sup>) and mass absorption cross sections (MAC, m<sup>b</sup> g<sup>-1</sup>) in different seasons.

Parameter <sup>a</sup>	Annual		Pre-monsoon <sup>d</sup>		Monsoon <sup>d</sup>		Post-monsoon <sup>d</sup>		Winter <sup>d</sup>	
	AVE <sup>b</sup>	SD <sup>c</sup>	AVE	SD	AVE	SD	AVE	SD	AVE	SD
$b_{\text{abs-measured}, 405}$	7.13	9.16	13.39	18.38	3.42	1.72	8.91	3.89	8.07	3.84
$b_{\text{abs, non-dust, BC}, 405}$	3.50	5.55	7.51	11.55	1.86	1.06	4.26	1.94	2.93	1.48
$b_{\text{abs, non-dust, BrC}, 405}$	3.16	3.55	4.81	6.51	1.37	0.76	4.37	2.18	4.57	2.39
$b_{\text{abs-dust}, 405}$	0.54	0.66	1.06	1.17	0.25	0.27	0.28	0.15	0.58	0.24
MAC <sub>non-dust, BC, 405</sub>	6.07	2.82	6.36	4.60	6.56	2.41	6.17	1.61	4.92	1.81
MAC <sub>non-dust, BrC, 405</sub>	0.72	0.55	0.74	0.41	0.33	0.18	1.06	0.57	1.26	0.53
$b_{\text{abs-measured}, 445}$	4.53	5.99	8.73	12.16	2.23	1.13	5.85	2.30	4.78	2.20
$b_{\text{abs, non-dust, BC}, 445}$	3.24	5.18	7.17	10.97	1.70	1.00	3.88	1.76	2.67	1.35
$b_{\text{abs, non-dust, BrC}, 445}$	1.11	1.07	1.43	1.67	0.45	0.26	1.77	0.83	1.69	0.91
$b_{\text{abs-dust}, 445}$	0.41	0.50	0.79	0.88	0.19	0.21	0.21	0.11	0.44	0.18
MAC <sub>non-dust, BC, 445</sub>	5.31	2.83	5.29	4.56	5.72	2.63	5.62	1.46	4.48	1.64
MAC <sub>non-dust, BrC, 445</sub>	0.25	0.22	0.23	0.20	0.10	0.08	0.42	0.18	0.47	0.20
$b_{\text{abs-measured}, 635}$	2.39	3.74	5.18	7.73	1.25	0.71	2.92	1.29	2.01	1.03
$b_{\text{abs, non-dust, BC}, 635}$	2.23	3.54	4.78	7.38	1.19	0.67	2.72	1.24	1.87	0.94
$b_{\text{abs, non-dust, BrC}, 635}$	0.04	0.07	0.05	0.12	0.02	0.03	0.10	0.07	0.05	0.04
$b_{\text{abs-dust}, 635}$	0.14	0.17	0.27	0.30	0.06	0.07	0.07	0.04	0.15	0.06
MAC <sub>non-dust, BC, 635</sub>	3.86	1.81	4.02	2.96	4.18	1.53	3.94	1.03	3.14	1.15
MAC <sub>non-dust, BrC, 635</sub>	0.01	0.02	0.02	0.04	0.00	0.01	0.02	0.02	0.01	0.01
$b_{\text{abs-measured}, 780}$	1.96	2.91	4.18	6.00	1.06	0.57	2.29	0.98	1.68	0.79
$b_{\text{abs, non-dust, BC}, 780}$	1.82	2.88	3.90	6.00	0.97	0.55	2.21	1.01	1.52	0.77
$b_{\text{abs, non-dust, BrC}, 780}$	0.01	0.02	0.02	0.05	0.00	0.01	0.02	0.02	0.01	0.01
$b_{\text{abs-dust}, 780}$	0.07	0.09	0.14	0.16	0.03	0.04	0.04	0.02	0.08	0.03
MAC <sub>non-dust, BC, 780</sub>	3.15	1.47	3.30	2.39	3.41	1.25	3.21	0.83	2.56	0.94
MAC <sub>non-dust, BrC, 780</sub>	0.00	0.01	0.01	0.01	0.00	0.00	0.01	0.01	0.00	0.00
$b_{\text{abs-measured}, 808}$	1.81	2.75	3.87	5.69	0.97	0.57	2.13	0.94	1.53	0.73
$b_{\text{abs, non-dust, BC}, 808}$	1.76	2.81	3.77	5.79	0.92	0.54	2.14	0.97	1.47	0.74
$b_{\text{abs, non-dust, BrC}, 808}$	0.01	0.02	0.01	0.04	0.00	0.01	0.02	0.02	0.01	0.01
$b_{\text{abs-dust}, 808}$	0.07	0.08	0.13	0.14	0.03	0.03	0.03	0.02	0.07	0.03
MAC <sub>non-dust, BC, 808</sub>	3.01	1.46	3.19	2.31	3.21	1.34	3.09	0.81	2.47	0.91
MAC <sub>non-dust, BrC, 808</sub>	0.00	0.01	0.00	0.01	0.00	0.00	0.00	0.01	0.00	0.00

<sup>a</sup> Abbreviations: BC stands for black carbon and BrC stands for brown carbon. The three-digit number is wavelength in nm.<sup>b</sup> AVE: arithmetic mean.<sup>c</sup> SD: standard deviation.<sup>d</sup> Pre-monsoon (Feb. 18–Apr. 27, 2009), monsoon (Jul. 16–Oct. 3, 2008; Apr. 28–Aug. 26, 2009), post-monsoon (Oct. 4–Nov. 9, 2008) and winter (Nov. 10, 2008–Feb. 17, 2009).

Kruskal-Wallis tests of the MAC<sub>non-dust, BC, 405</sub> values did not show significant differences (asymptotic significance levels of 0.363 as compared with a level of significance of < 0.05) for the data stratified by season. The MAC<sub>non-dust, BrC, 405</sub> values were found to be highly variable. Kruskal-Wallis Tests showed significant differences (asymptotic significance level < 0.001) across the MAC<sub>non-dust, BrC, 405</sub> in different seasons. The MAC<sub>non-dust, BrC, 405</sub> increased from 0.3 m<sup>2</sup> g<sup>-1</sup> in the monsoon to 1.1 m<sup>2</sup> g<sup>-1</sup> in the post-monsoon and 1.3 m<sup>2</sup> g<sup>-1</sup> in winter, then gradually decreased to ~0.7 m<sup>2</sup> g<sup>-1</sup> in the pre-monsoon. Results indicate that organic aerosol in winter and post-monsoon absorbs UV-visible light more efficiently than those in monsoon.

The low MAC<sub>non-dust, BrC, 405</sub> values during the monsoon may be related to the emission of plant spores and pollen as well as the formation of SOC during times of high atmospheric OC. To investigate this possibility, SOC was estimated through an EC-tracer method (Turpin and Huntzicker, 1995) which makes use of the following equation:

$$\text{SOC} = \text{OC} - \text{BC} (\text{OC}/\text{BC})_{\text{min}}$$

where OC is the total average OC by season and (OC/BC)<sub>min</sub> is the minimum ratio observed in each corresponding season. The SOC fractions of OC were found to be 69.3% in the monsoon, but lower (29%–33%) during the other seasons. High temperatures and intense solar radiation during the monsoon can provide conditions favorable for the photochemical production of SOC, leading to the lowest MAC<sub>non-dust, BrC, 405</sub>. Similar seasonal fluctuations of MAC<sub>non-dust, BrC, 405</sub> and comparable MAC<sub>WSOC, 365</sub> values obtained from water-based extractions were observed at Lulang (0.84 ± 0.40 m<sup>2</sup> g<sup>-1</sup>) and the Everest station (1.18 ± 0.64 m<sup>2</sup> g<sup>-1</sup>), which is located on the northern slope of the middle Himalayas (Li et al., 2016b).

The non-dust  $b_{\text{abs}}$  and MAC values of BC versus BrC were well correlated in winter and the pre-monsoon ( $r^2$  ranged from 0.57 to 0.83,  $p < 0.001$ , Fig. 3). This implies that BC and BrC shared the same primary sources at those times, most likely biomass burning, fossil fuel combustion, etc. More to the point, similarities in production and transport evidently caused the light absorption characteristics of BC and BrC to covary in those two seasons. In contrast, relatively low correlations ( $r^2$  ranged from 0.1 to 0.38) between these variables during the monsoon and post-monsoon suggest that some sources that affected BrC (e.g., biogenic emission, secondary formation, etc.) were not necessarily linked with BC. In addition, the average MAC<sub>non-dust, BrC</sub>/MAC<sub>non-dust, BC</sub> ratio in winter (0.26 ± 0.06) was twice as high as that in the pre-monsoon (0.13 ± 0.06), which may have been caused by seasonal differences in the main emission sources, as well as BC aging processes, or BrC loss mechanisms. For example, the aerosol in pre-monsoon might be more impacted by long-range transport from South Asia while that in winter might be more influenced by local emission sources. Indeed, Li et al. (2016b) speculated that BrC losses through chemical bleaching or evaporation during long-range transport from source regions to Lulang in the pre-monsoon, led to relatively low MAC<sub>BrC</sub> values during that season. However, more studies are needed to understand the mechanisms involved in BrC processing and aging.

#### 4.3. Absorption Ångström exponent ( $\alpha$ )

The power-law relationships between  $b_{\text{abs, non-dust}}$  and wavelength showed high correlations (0.95 <  $r^2$  < 0.97) with apparent increases in  $b_{\text{abs}}$  at lower wavelengths (Olson et al., 2015; Ran et al., 2016). Fig. 4 shows  $\alpha_{\text{aerosol}, 405-808}$  increased from a low value of 1.55 in the pre-

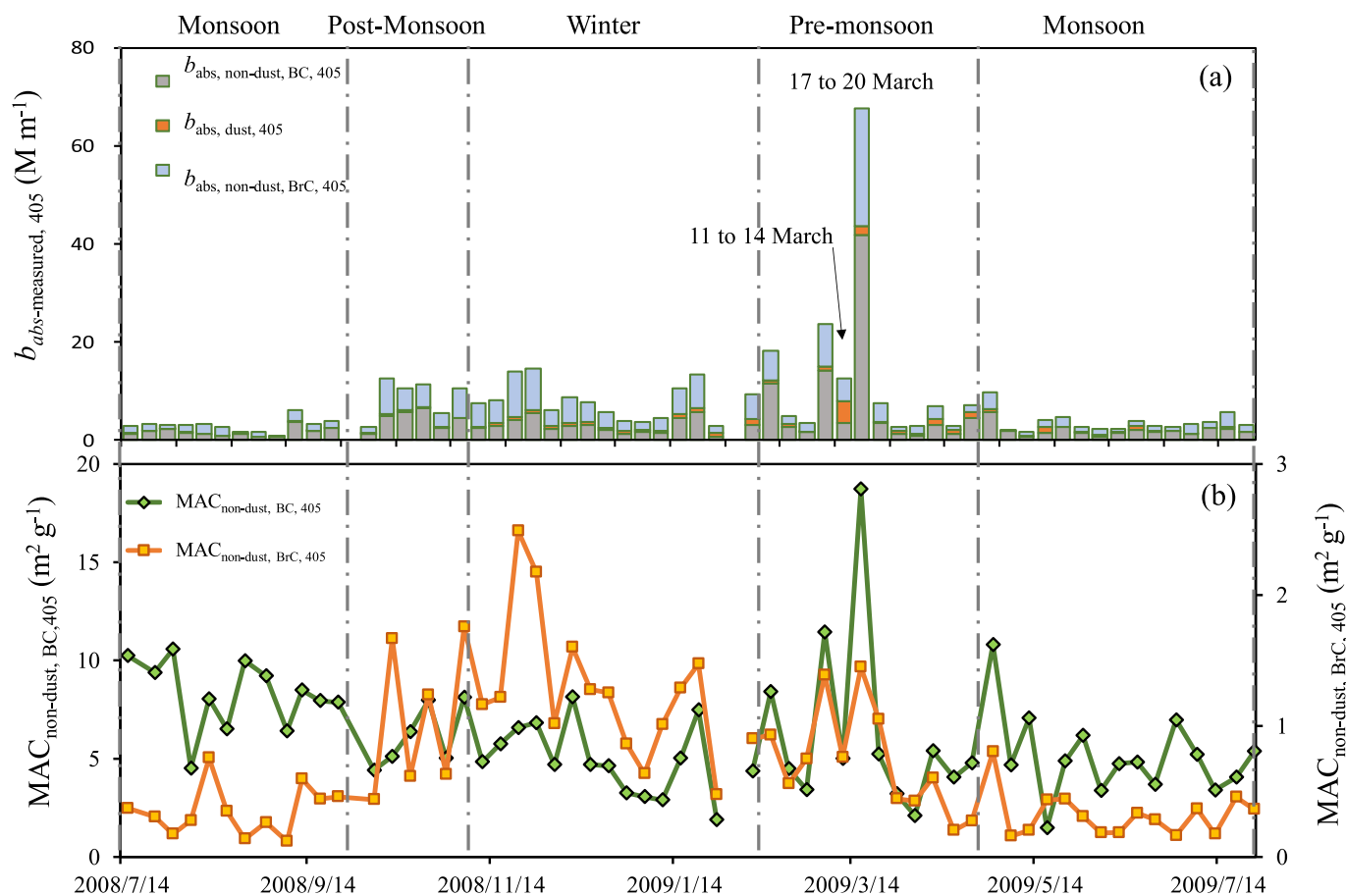


Fig. 2. (a) Attribution of total aerosol light absorption ( $b_{abs-measured}$ ) at 405 nm, assuming an absorption Ångström exponent for black carbon of unity, and (b) temporal variations of mass absorption cross sections of brown carbon and black carbon ( $MAC_{non-dust, BrC, 405}$ , and  $MAC_{non-dust, BC, 405}$ , respectively). (For interpretation of the references to colour in this figure legend, the reader is referred to the Web version of this article.)

monsoon, increased to 1.61 in monsoon, 1.92 in post-monsoon, to 2.19 in winter (Fig. 4, red solid lines), again attests to the presence of non-BC light-absorbing components throughout the year. Despite the fact that substantially stronger absorption was observed in the pre-monsoon compared with other seasons, some high  $\alpha_{aerosol, 405-808}$  values were found in the post-monsoon and winter. Fig. 2 also shows the  $b_{abs, non-dust}$  for BC (black dashed line) and BrC (green dashed line) at different wavelengths. The contribution of  $b_{abs, non-dust, BrC}$  to the total non-dust absorption was inversely related to wavelength, and at long wavelengths, especially  $> 635$  nm,  $b_{abs, non-dust, BrC}$  was negligible ( $\sim 1$ –4%). The  $\alpha_{non-dust, BrC}$  values were similar for the pre-monsoon (15.0) and monsoon (14.0) and decreased by  $\sim 35\%$  in winter and the post-monsoon (10.7 and 9.7, respectively).

Elevated  $\alpha_{non-dust, BrC}$  but the lowest  $\alpha_{aerosol, 405-808}$  values in the pre-monsoon implies impacts from biomass burning, and this assertion is supported by the observed high levels of levoglucosan ( $33.3 \pm 49.8$  ng  $m^{-3}$ ). Increased biomass burning emissions produced not only BrC but also BC, which was consistent with the high measured levels of BC. For the relatively high  $\alpha_{non-dust, BrC}$  values during the monsoon, we speculated that impacted from photochemically-produced fresh SOC. BONES et al. (2010) showed that SOC was an important contributor to BrC, and furthermore, the  $\alpha$  of fresh SOC-BrC ( $\sim 8.6$ –17.8) was much higher than that of aged SOC ( $\sim 4.7$ –5.3). Thus, the  $\alpha_{non-dust, BrC}$  values during the monsoon were likely influenced by more photochemically-produced fresh SOC. In contrast, the relatively low  $\alpha_{non-dust, BrC}$  values in the post-monsoon and winter were likely impacted by multiple sources. This point could be verified by PAHs, important anthropogenic components of organic aerosol, emitted from incomplete combustion of biomass and fossil fuels. Literature showed

that some PAHs are strongly light-absorbing compounds at near-UV wavelength range and therefore have been suggested to be important BrC chromophores (Huang et al., 2018; Samburova et al., 2016; Sun et al., 2007). Previous work carried on the same samples (Chen et al., 2014), using diagnostic ratios method (Flu/(Flu + Pyr) versus IcdP/(IcdP + BghiP)), revealed complex PAHs emission sources in post-monsoon (including wood, coal and grass burning as well as fossil fuel combustion sources).

The Lulang sampling site is situated in Linzhi Prefecture, which is surrounded by extensive forests. BVOCs (like isoprene, lignin pyrolysis products) emitted from the large forests in growing season could act as precursors, then generate BrC through heterogeneous or multiphase reactions (Laskin et al., 2015). And the strong solar radiation Tibetan Plateau may also accelerate the formation of BrC through the photochemical reactions (Wu et al., 2016). In monsoon, levoglucosan concentration is relatively low ( $5$  ng  $m^{-3}$ ; levoglucosan in most samples cannot be detected), indicating less impact from biomass burning emissions. However, the  $b_{abs, non-dust, BrC, 405}$  still contributed nearly  $\sim 40\%$  to the total light absorption, which might impact from the great amount emission of BVOCs. In addition, Li et al. (2016a) found equal contributions from fossil fuel ( $46 \pm 11\%$ ) and biomass ( $54 \pm 11\%$ ) combustion for the Himalayas, whereas BC in the remote northern TP predominantly derives from fossil fuel combustion ( $66 \pm 16\%$ ). Therefore, by combing these two factors together, BrC could be more easily formed in southeast TP than other areas in TP all the year round. In other words, light absorption characteristics might exhibit large differences among various regions in TP.

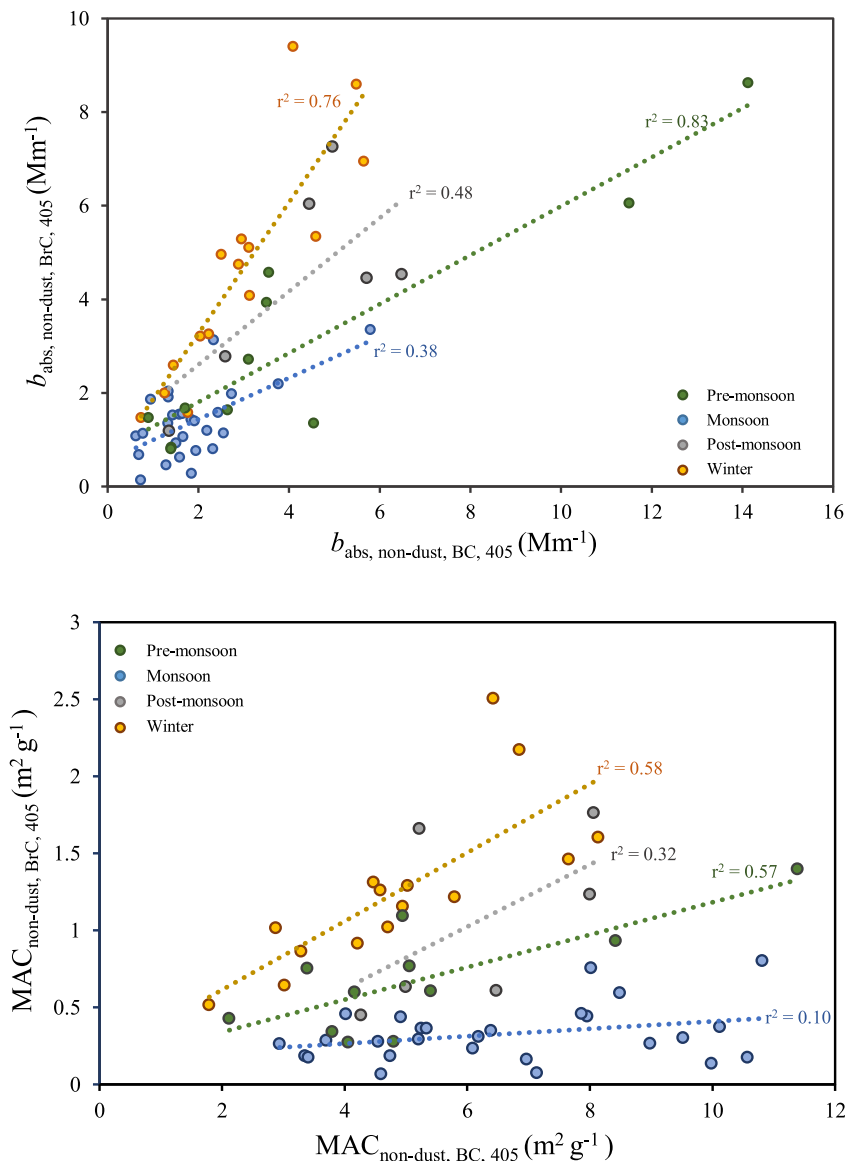


**Fig. 3.** (a) Non-dust aerosol light absorption values for brown versus black carbon ( $b_{\text{abs, non-dust, BC, 405}}$  versus  $b_{\text{abs, non-dust, BrC, 405}}$ ) and (b) mass absorption cross sections for brown carbon versus black carbon ( $\text{MAC}_{\text{non-dust, BC, 405}}$  versus  $\text{MAC}_{\text{non-dust, BrC, 405}}$ ) in four seasons. (The data of the pollution episode on 17 to 20 March 2009 in pre-monsoon was removed from the regression due to extremely high). (For interpretation of the references to colour in this figure legend, the reader is referred to the Web version of this article.)

#### 4.4. Relative contributions of BC and BrC to radiative forcing

The fractional contributions of solar absorption by BrC relative to BC integrated over wavelengths of 405–808 nm were estimated from Eq. (11). The mean value of the BrC versus BC relative absorption was  $29.4 \pm 9.5\%$  (range: 10%–45%); the proportions were relatively high (~30%–40%) in winter and pre-monsoon months (i.e., from October to March); and compared with BC, the BrC contributions were more variable during the warmer seasons (Fig. 5). Seasonal averages of the relative radiative BrC/BC forcing were not significant, decreased from 35.5% in winter to 33.4% in the post-monsoon to 29.8% in the pre-monsoon, and 24.9% in the monsoon. In previous studies, BrC extracted with water (WS–BrC) or methanol (MeS–BrC) were measured to estimate the absorption of BrC relative to BC in Himalayas, the Tibetan Plateau, and South Asia (Kirillova et al., 2014b, 2016; Li et al., 2016b; Srinivas et al., 2016; Srinivas and Sarin, 2014). In comparison, the results from the present study were higher than those for the Nepal Climate Observatory-Pyramid (NCO-P) station in the southern Himalayas

(8% for WS–BrC and 17% for MeS–BrC), but they were comparable with those from ambient aerosols from the Indo-Gangetic Plain (35% and 40% for WS–BrC in daytime and nighttime) (Srinivas et al., 2016). Much lower BrC light absorption at the Lulang site was reported by (Li et al., 2016b), and these authors found that the fractional solar radiation absorption by WS–BrC was only 6% of that by BC. One possible cause for the discrepancy between our study and theirs is that only WSOC was measured by Li et al. (2016a, b), and other light absorbing components, such as water-insoluble organic carbon ((Bond and Bergstrom, 2006), were not included in their assessment and analysis.

#### 4.5. Uncertainty assessment and limitations

Lack and Langridge (2013) pointed out that absorption Ångström exponent attribution methods for assessing the contributions of BC and BrC to absorption are sensitive to the choice of  $\alpha$ . That is, the uncertainty ranges of  $\alpha$  for BC need to be considered and propagated through BrC and BC absorption attribution calculations. Thus, special

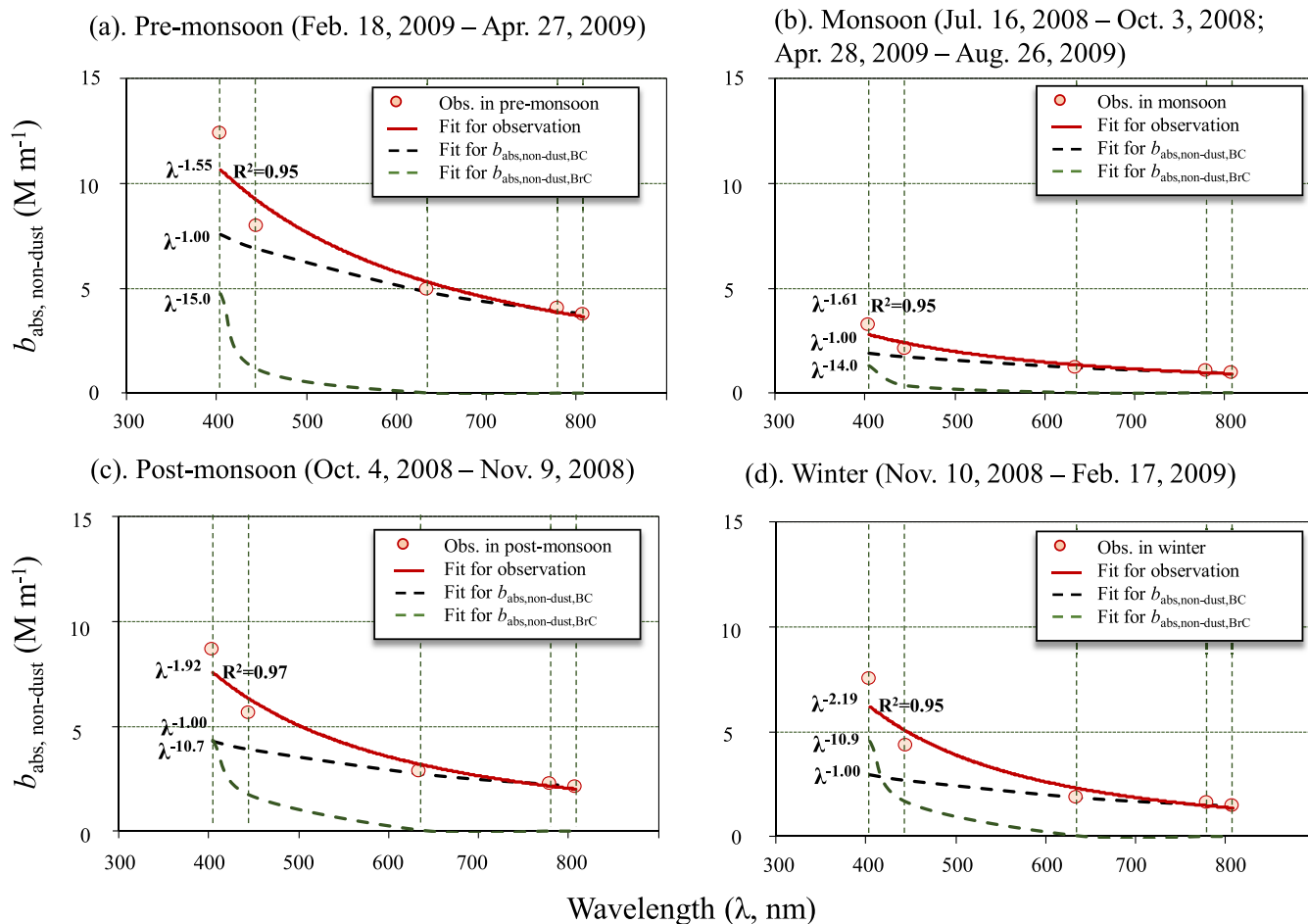


**Fig. 4.** Average absorption coefficients for non-dust aerosol ( $b_{\text{abs,non-dust}}$ ) at five wavelengths (405, 445, 635, 780, and 808 nm) for each season (red dots). Power law relationships (red solid lines) fitted based on Equation (7). The black and green dashed lines show the wavelength-dependent  $b_{\text{abs,non-dust}}$  apportioned into black carbon (BC) and brown carbon (BrC), based on a two-component model. (For interpretation of the references to colour in this figure legend, the reader is referred to the Web version of this article.)

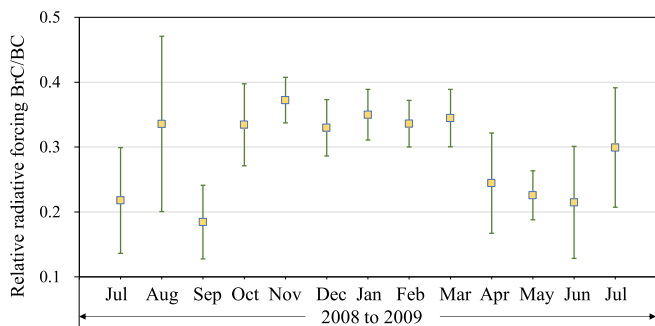


**Fig. 5.** Fractional solar radiation absorption by brown carbon (BrC) relative to black carbon (BC) at Lulang throughout the year. (For interpretation of the references to colour in this figure legend, the reader is referred to the Web version of this article.)

care needs to be taken in interpreting the apportioning results. A series of field measurements revealed that  $\alpha_{\text{BC}}$  typically ranged from 0.8 to 1.4 (Lack and Langridge, 2013), which we cited here in separate calculations. The variability of  $b_{\text{abs, non-dust}}$  apportionment and  $\alpha_{\text{BrC,405–808}}$  results for different seasons are listed in Table S2. When the  $\alpha_{\text{BC}}$  set as 0.8, compared to the  $\alpha_{\text{BC}} = 1$ , the  $\alpha_{\text{BrC,405–808}}$  decreased from -7% to -18% in different seasons. The  $b_{\text{abs,non-dust,BC}}$  decreased -11.13% at 405 nm, -9.43% at 445 nm, -2.6% at 635 nm. Correspondingly, the annual averaged  $b_{\text{abs,non-dust,BC}}$  contribution to  $b_{\text{abs,non-}}$

dust at 405 nm dropped from 52.4% to 46.6%. When the  $\alpha_{\text{BC}}$  set as 1.4, the calculated  $b_{\text{abs,non-dust,BC}}$  increased +22.1% at 405 nm, 17.61% at 445 nm to 2.07% at 635 nm. Due to the extremely low contribution of BrC to  $b_{\text{abs}}$  at 780 nm and 808 nm, the variability in  $b_{\text{abs,non-dust, BC}}$  and  $b_{\text{abs,non-dust, BrC}}$  were not significant. By combining those uncertainties with Model\_2015 OCEC analyzer measurement errors (here we assuming as a constant value  $\pm 5\%$ ), the relative uncertainties of BC and BrC absorption can be estimated by equations S1 and S2. A detailed description of the relative uncertainties in  $b_{\text{abs,BC}}$  and  $b_{\text{abs, BrC}}$  could be found in Text S2 in supplement. The relative uncertainties of  $b_{\text{abs-BC}}$  ( $U_{b_{\text{abs-BC}}}$ ) were estimated to be [-14.7%, +28.1%] at 405 nm, [-12.9%, +24.4%] at 445 nm, [-6.9%, +10.9%] at 635 nm, [-5.1%, +5.2%] at 780 nm, and [-5, +5%] at 808 nm. After  $U_{b_{\text{abs-BC}}}$  estimated, the relative uncertainty associated with derived BrC absorption ( $U_{b_{\text{abs-BrC}}}$ ) can be assessed following the equation (S2), which were calculated to be [-32.6%, +55.3%] at 405 nm, [-44.7%, +77.9%] at 445 nm, [-2.2%, +3.0%] at 635 nm.

The study does have some limitations that should be acknowledged. First, systematic biases (e.g. loading effects, multiple scattering and shadow effects) are inherent to filter-based methods and Instruments used for studying light absorption by aerosols. According to Chow et al. (2018), due to saturation effects of laser response, as EC concentrations increase, the ATN showed a gradual reduction. For high EC concentrations (e.g.,  $\text{EC} > 0.65 \mu\text{g m}^{-3}$  in that study), the measured ATN and Absorption Ångström exponents represent a lower bound of the actual values. And the loading effects is more pronounced at shorter

wavelengths owing to higher BC absorption as well as the presence of BrC. Thus, loading corrections similar to those applied to the aethalometer could be investigated to increase ATN accuracy at high EC concentrations. Second, the dust loadings in the samplers may have influenced the laser baselines during analysis to some extent. Although some corrections for ATN and ABS were made, there remain some uncertainties in the calculations. In particular, the relationships between ATN and  $b_{\text{abs}}$  might depend on filter thickness, and how deep the particles penetrate into the filter, thus the factors that drive those relationships require additional research.

## 5. Summary and conclusions

Light absorption characteristics and seasonal variations of BC and BrC in TSP collected from the Lulang site on the southeast TP were studied. Clear seasonal variations of  $b_{\text{abs}}$  were observed, with the highest aerosol absorption during pre-monsoon followed in decreasing order by the post-monsoon, winter, and monsoon. The seasonally-averaged absorption angstrom exponents ( $\alpha_{\text{non-dust, BrC, 405-808}}$ ) decreased as follows: pre-monsoon > monsoon > winter > post-monsoon. The  $\alpha_{\text{aerosol}}$  values were lowest in pre-monsoon and highest in winter, presumably due to the intensive biomass burning in upwind areas during the colder parts of the year. The grand mean  $\text{MAC}_{\text{non-dust, BC}}$  and  $\text{MAC}_{\text{non-dust, BrC}}$  values at 405 nm were  $6.1 \pm 2.9 \text{ m}^2 \text{ g}^{-1}$  and  $0.72 \pm 0.54 \text{ m}^2 \text{ g}^{-1}$ . Nonparametric Kruskal-Wallis tests indicate that  $\text{MAC}_{\text{non-dust, BC, 405}}$  was relatively constant but larger seasonal variability was found for  $\text{MAC}_{\text{non-dust, BrC, 405}}$ . Correlations between non-dust  $b_{\text{abs}}$  and MAC values of BC versus BrC in four seasons suggesting that BrC shared the same primary sources with BC in pre-monsoon and winter, but a mixture of sources impacted BrC in monsoon and post-monsoon. The relative contributions of radiative forcing of BrC relative to BC integrated over wavelengths of 405 nm–808 nm were ~35.5% winter, 33.4% in post-monsoon, 29.8% in pre-monsoon, and 24.9% in monsoon, confirming the importance of BrC for light absorption in the near UV throughout the year. The results are important because the study demonstrates the ubiquitous presence of BrC over the southeast TP. The presence of BrC and BC at the observed concentrations would be sufficient to cause decreases in the flux of solar radiation, reduce surface radiative forcing, and possibly influence circulation patterns. Therefore, the sources, cycling, and combined effects of all light-absorbing aerosol species need to be considered in the development of climate models.

## Acknowledgements

This study was supported by the National Natural Science Foundation of China (41603129, 21661132005, 41877391) and West Light Foundation of The Chinese Academy of Sciences (XAB2015B02). Qiyuan Wang also acknowledged the support of the Youth Innovation Promotion Association CAS.

## Appendix A. Supplementary data

Supplementary data to this article can be found online at <https://doi.org/10.1016/j.atmosenv.2019.05.035>.

## References

Andreae, M.O., Gelencsér, A., 2006. Black carbon or brown carbon? The nature of light-absorbing carbonaceous aerosols. *Atmos. Chem. Phys.* 6, 3131–3148.

Arnott, W.P., Hamasha, K., Moosmüller, H., Sheridan, P.J., Ogren, J.A., 2005. Towards aerosol light-absorption measurements with a 7-wavelength Aethalometer: evaluation with a photoacoustic instrument and 3-wavelength nephelometer. *Aerosol Sci. Technol.* 39, 17–29.

Bahadur, R., Praveen, P.S., Xu, Y., Ramanathan, V., 2012. Solar absorption by elemental and brown carbon determined from spectral observations. *Proc. Natl. Acad. Sci. U.S.A.* 109, 17366–17371.

Bernardini, V., Pileci, R.E., Caponi, L., Massabò, D., 2017. The multi-wavelength

Absorption analyzer (MWA) model as a tool for source and component apportionment based on aerosol absorption properties: application to samples collected in different environments. *Atmosphere* 8, 218.

Bonasoni, P., Laj, P., Marinoni, A., Sprenger, M., Angelini, F., Arduini, J., Bonafè, U., Calzolari, F., Colombo, T., Decesari, S., Di Biagio, C., di Sarra, A.G., Evangelisti, F., Duchi, R., Facchini, M.C., Fuzzi, S., Gobbi, G.P., Maione, M., Panday, A., Roccatò, F., Sellegri, K., Venzac, H., Verza, G.P., Villani, P., Vuillermoz, E., Cristofanelli, P., 2010. Atmospheric Brown Clouds in the Himalayas: first two years of continuous observations at the Nepal Climate Observatory-Pyramid (5079 m). *Atmos. Chem. Phys.* 10, 7515–7531.

Bond, T.C., Bergstrom, R.W., 2006. Light absorption by carbonaceous particles: an investigative review. *Aerosol Sci. Technol.* 40, 27–67.

Bond, T.C., Doherty, S.J., Fahey, D.W., Forster, P.M., Bernsten, T., DeAngelo, B.J., Flanner, M.G., Ghan, S., Kärcher, B., Koch, D., Kinne, S., Kondo, Y., Quinn, P.K., Sarofim, M.C., Schultz, M.G., Schulz, M., Venkataraman, C., Zhang, H., Zhang, S., Bellouin, N., Guttikunda, S.K., Hopke, P.K., Jacobson, M.Z., Kaiser, J.W., Klimont, Z., Lohmann, U., Schwarz, J.P., Shindell, D., Storelvmo, T., Warren, S.G., Zender, C.S., 2013. Bounding the role of black carbon in the climate system: a scientific assessment. *J. Geophys. Res.: Atmosphere* 118 5380–5552.

Bones, D.L., Henricksen, D.K., Mang, S.A., Gonsior, M., Bateman, A.P., Nguyen, T.B., Cooper, W.J., Nizkorodov, S.A., 2010. Appearance of strong absorbers and fluorophores in limonene-O3 secondary organic aerosol due to  $\text{NH}_4^+$ -mediated chemical aging over long time scales. *J. Geophys. Res.: Atmosphere* 115, 1–14.

Cao, J.J., Tie, X.X., Xu, B.Q., Zhao, Z.Z., Zhu, C.S., Li, G.H., Liu, S.X., 2010. Measuring and modeling black carbon (BC) contamination in the SE Tibetan Plateau. *J. Atmos. Chem.* 67, 45–60.

Caponi, L., Formenti, P., Massabò, D., Di Biagio, C., Cazaunau, M., Pangui, E., Chevaillier, S., Landrot, G., Andreae, M.O., Kandler, K., Piketh, S., Saeed, T., Seibert, D., Williams, E., Balkanski, Y., Prati, P., Doussin, J.F., 2017. Spectral- and size-resolved mass absorption efficiency of mineral dust aerosols in the shortwave spectrum: a simulation chamber study. *Atmos. Chem. Phys.* 17, 7175–7191.

Chen, L.W.A., Chow, J.C., Wang, X.L., Robles, J.A., Sunlin, B.J., Lowenthal, D.H., Zimmermann, R., Watson, J.G., 2015. Multi-wavelength optical measurement to enhance thermal/optical analysis for carbonaceous aerosol. *Atmos. Meas. Tech.* 8, 451–461.

Chen, Y., Cao, J.J., Zhao, J., Xu, H.M., Arimoto, R., Wang, G.H., Han, Y.M., Shen, Z.X., Li, G.H., 2014. n-Alkanes and polycyclic aromatic hydrocarbons in total suspended particulates from the southeastern Tibetan Plateau: concentrations, seasonal variations, and sources. *Sci. Total Environ.* 470, 9–18.

Chow, J.C., Wang, X., Sunlin, B.J., Gronstal, S.B., Chen, A.L.-W., Trimble, D.L., Kohl, S.D., Mayorga, S.R., Riggio, G., Hurbain, P.R., Johnson, M., Zimmermann, R., Watson, J.G., 2015. Optical calibration and equivalence of a multiwavelength thermal/optical carbon analyzer. *Aerosol Air Qual. Res.* 15, 1145–1159.

Chow, J.C., Watson, J.G., Chen, L.W.A., Arnott, W.P., Moosmüller, H., Fung, K., 2004. Equivalence of elemental carbon by thermal/optical reflectance and transmittance with different temperature protocols. *Environ. Sci. Technol.* 38, 4414–4422.

Chow, J.C., Watson, J.G., Chen, L.W.A., Chang, M.C.O., Robinson, N.F., Trimble, D., Kohl, S., 2007. The IMPROVE-A temperature protocol for thermal/optical carbon analysis: maintaining consistency with a long-term database. *J. Air Waste Manag. Assoc.* 57, 1014–1023.

Chow, J.C., Watson, J.G., Green, M.C., Wang, X., Chen, L.W.A., Trimble, D.L., Cropper, P.M., Kohl, S.D., Gronstal, S.B., 2018. Separation of brown carbon from black carbon for IMPROVE and Chemical Speciation Network PM2.5 samples. *J. Air Waste Manag. Assoc.* 68, 494–510.

Chow, J.C., Watson, J.G., Robles, J., Wang, X., Chen, L.W.A., Trimble, D.L., Kohl, S.D., Tropp, R.J., Fung, K.K., 2011. Quality assurance and quality control for thermal/optical analysis of aerosol samples for organic and elemental carbon. *Anal. Bioanal. Chem.* 401, 3141–3152.

Coen, M.C., Weingartner, E., Apituley, A., Ceburnis, D., Fierz-Schmidhauser, R., Flentje, H., Henzing, J.S., Jennings, S.G., Moerman, M., Petzold, A., Schmid, O., Baltensperger, U., 2010. Minimizing light absorption measurement artifacts of the Aethalometer: evaluation of five correction algorithms. *Atmos. Meas. Tech.*

Eklund, A.G., Chow, J.C., Greenbaum, D.S., Hidy, G.M., Kleinman, M.T., Watson, J.G., Wyzga, R.E., 2014. Public health and components of particulate matter: the changing assessment of black carbon. *J. Air Waste Manag. Assoc.* 64, 1221–1231.

Feng, Y., Ramanathan, V., Kotamarthi, V.R., 2013. Brown carbon: a significant atmospheric absorber of solar radiation? *Atmos. Chem. Phys.* 13, 8607–8621.

Gertler, C.G., Puppala, S.P., Panday, A., Stumm, D., Shea, J., 2016. Black carbon and the Himalayan cryosphere: a review. *Atmos. Environ.* 125, 404–417.

Gustafsson, Ö., Kruså, M., Zencak, Z., Sheesley, R.J., Granat, L., Engström, E., Praveen, P.S., Rao, P.S.P., Leck, C., Rodhe, H., 2009. Brown clouds over south Asia: biomass or fossil fuel combustion? *Science* 323, 495–498.

Han, Y.M., Lee, S.C., Cao, J.J., Ho, K.F., An, Z.S., 2009. Spatial distribution and seasonal variation of char-EC and soot-EC in the atmosphere over China. *Atmos. Environ.* 43, 6066–6073.

Hansen, A.D.A., Rosen, H., Novakov, T., 1984. The Aethalometer— an instrument for the real-time measurement of optical absorption by aerosol particles. *Sci. Total Environ.* 36, 191–196.

Healy, R.M., Sofowote, U., Su, Y., Deboz, J., Noble, M., Jeong, C.H., Wang, J.M., Hilker, N., Evans, G.J., Doerksen, G., Jones, K., Munoz, A., 2017. Ambient measurements and source apportionment of fossil fuel and biomass burning black carbon in Ontario. *Atmos. Environ.* 161, 34–47.

Hu, Z., Kang, S., Li, C., Yan, F., Chen, P., Gao, S., Wang, Z., Zhang, Y., Sillanpää, M., 2017. Light absorption of biomass burning and vehicle emission-sourced carbonaceous aerosols of the Tibetan Plateau. *Environ. Sci. Pollut. Control Res.* 24, 15369–15378.

Huang, R.-J., Yang, L., Cao, J., Chen, Y., Chen, Q., Li, Y., Duan, J., Zhu, C., Dai, W., Wang,

- K., Lin, C., Ni, H., Corbin, J.C., Wu, Y., Zhang, R., Tie, X., Hoffmann, T., O'Dowd, C., Dusek, U., 2018. Brown carbon aerosol in urban xi'an, northwest China: the composition and light absorption properties. *Environ. Sci. Technol.* 52, 6825–6833.
- Jimenez, J., Claiborn, C., Larson, T., Gould, T., Kirchstetter, T.W., Gundel, L., 2007. Loading effect correction for real-time aethalometer measurements of fresh diesel soot. *J. Air Waste Manag. Assoc.* 57, 868–873.
- Jo, D.S., Park, R.J., Lee, S., Kim, S.W., Zhang, X., 2016. A global simulation of brown carbon: implications for photochemistry and direct radiative effect. *Atmos. Chem. Phys.* 16, 3413–3432.
- Kirillova, E.N., Andersson, A., Han, J., Lee, M., Gustafsson, Ö., 2014a. Sources and light absorption of water-soluble organic carbon aerosols in the outflow from northern China. *Atmos. Chem. Phys.* 14, 1413–1422.
- Kirillova, E.N., Andersson, A., Tiwari, S., Srivastava, A.K., Bisht, D.S., Gustafsson, Ö., 2014b. Water-soluble organic carbon aerosols during a full New Delhi winter: isotope-based source apportionment and optical properties. *J. Geophys. Res.: Atmosphere* 119, 3476–3485.
- Kirillova, E.N., Marinoni, A., Bonasoni, P., Vuilleumoz, E., Facchini, M.C., Fuzzi, S., Decesari, S., 2016. Light absorption properties of brown carbon in the high Himalayas. *J. Geophys. Res.: Atmosphere* 121, 9621–9639.
- Lüthi, Z.L., Bojan, S., Kim, S.W., Lauer, A., Mues, A., Rupakheti, M., Kang, S., 2015. Atmospheric brown clouds reach the Tibetan Plateau by crossing the Himalayas. *Atmos. Chem. Phys.* 4, 28105–28146.
- Lack, D.A., Cappa, C.D., 2010. Impact of brown and clear carbon on light absorption enhancement, single scatter albedo and absorption wavelength dependence of black carbon. *Atmos. Chem. Phys.* 10, 4207–4220.
- Lack, D.A., Langridge, J.M., 2013. On the attribution of black and brown carbon light absorption using the Ångström exponent. *Atmos. Chem. Phys.* 13, 10535–10543.
- Laskin, A., Laskin, J., Nizkorodov, S.A., 2015. Chemistry of atmospheric Brown carbon. *Chem. Rev.* 115, 4335–4382.
- Levinson, R., Akbari, H., Berdahl, P., 2010. Measuring solar reflectance—Part I: defining a metric that accurately predicts solar heat gain. *Sol. Energy* 84, 1717–1744.
- Li, C., Bosch, C., Kang, S., Andersson, A., Chen, P., Zhang, Q., Cong, Z., Chen, B., Qin, D., Gustafsson, O., 2016a. Sources of black carbon to the Himalayan-Tibetan Plateau glaciers. *Nat. Commun.* 7.
- Li, C., Kang, S., Yan, F., 2018. Importance of local black carbon emissions to the fate of glaciers of the third Pole. *Environ. Sci. Technol.* 52.
- Li, C., Kang, S., Zhang, Q., 2009. Elemental composition of Tibetan Plateau top soils and its effect on evaluating atmospheric pollution transport. *Environ. Pollut.* 157, 2261–2265.
- Li, C., Yan, F., Kang, S., Chen, P., Hu, Z., Gao, S., Qu, B., Sillanpää, M., 2016b. Light absorption characteristics of carbonaceous aerosols in two remote stations of the southern fringe of the Tibetan Plateau, China. *Atmos. Environ.* 143, 79–85.
- Li, X., Kang, S., He, X., Qu, B., Tripathy, L., Jing, Z., Paudyal, R., Li, Y., Zhang, Y., Yan, F., Li, G., Li, C., 2017. Light-absorbing impurities accelerate glacier melt in the Central Tibetan Plateau. *Sci. Total Environ.* 587–588, 482–490.
- Lin, G., Penner, J.E., Flanner, M.G., Sillman, S., Xu, L., Zhou, C., 2014. Radiative forcing of organic aerosol in the atmosphere and on snow: effects of SOA and brown carbon. *J. Geophys. Res.: Atmosphere* 119, 7453–7476.
- Liu, S., Aiken, A.C., Gorkowski, K., Dubey, M.K., Cappa, C.D., Williams, L.R., Herndon, S.C., Massoli, P., Fortner, E.C., Chhabra, P.S., Brooks, W.A., Onasch, T.B., Jayne, J.T., Worsnop, D.R., China, S., Sharma, N., Mazzoleni, C., Xu, L., Ng, N.L., Liu, D., Allan, J.D., Lee, J.D., Fleming, Z.L., Mohr, C., Zotter, P., Szidat, S., Prevot, A.S.H., 2015. Enhanced light absorption by mixed source black and brown carbon particles in UK winter. *Nat. Commun.* 6.
- Marcq, S., Laj, P., Roger, J.C., Villani, P., Sellegri, K., Bonasoni, P., Marinoni, A., Cristofanelli, P., Verza, G.P., Bergin, M., 2010. Aerosol optical properties and radiative forcing in the high Himalaya based on measurements at the Nepal Climate Observatory-Pyramid site (5079m.a.s.l.). *Atmos. Chem. Phys.* 10, 5859–5872.
- Masiello, C.A., 2004. New directions in black carbon organic geochemistry. *Mar. Chem.* 92, 201–213.
- Massabò, D., Caponi, L., Bernardoni, V., Bove, M.C., Brotto, P., Calzolari, G., Cassola, F., Chiari, M., Fedi, M.E., Fermo, P., Giannoni, M., Lucarelli, F., Nava, S., Piazzalunga, A., Valli, G., Vecchi, R., Prati, P., 2015. Multi-wavelength optical determination of black and brown carbon in atmospheric aerosols. *Atmos. Environ.* 108, 1–12.
- Moosmüller, H., Chakrabarty, R.K., Arnott, W.P., 2009. Aerosol light absorption and its measurement: a review. *J. Quant. Spectrosc. Radiat. Transf.* 110, 844–878.
- Olson, M.R., Victoria Garcia, M., Robinson, M.A., Van Rooy, P., Diitenberger, M.A., Bergin, M., Schauer, J.J., 2015. Investigation of black and brown carbon multiple-wavelength-dependent light absorption from biomass and fossil fuel combustion source emissions. *J. Geophys. Res.: Atmosphere* 120, 6682–6697.
- Pöschl, U., 2003. Aerosol particle analysis: challenges and progress. *Anal. Bioanal. Chem.* 375, 30–32.
- Petzold, A., Schloesser, H., Sheridan, P.J., Arnott, W.P., Ogren, J.A., Virkkula, A., 2005. Evaluation of multiangle Absorption photometry for measuring aerosol light absorption. *Aerosol Sci. Technol.* 39, 40–51.
- Ramanathan, V., Li, F., Ramana, M.V., Praveen, P.S., Kim, D., Corrigan, C.E., Nguyen, H., Stone, E.A., Schauer, J.J., Carmichael, G.R., Adhikary, B., Yoon, S.C., 2007. Atmospheric brown clouds: hemispherical and regional variations in long-range transport, absorption, and radiative forcing. *J. Geophys. Res.: Atmosphere* 112, D22S21.
- Ran, L., Deng, Z.Z., Wang, P.C., Xia, X.A., 2016. Black carbon and wavelength-dependent aerosol absorption in the North China Plain based on two-year aethalometer measurements. *Atmos. Environ.* 142, 132–144.
- Rengarajan, R., Sarin, M.M., Sudheer, A.K., 2007. Carbonaceous and inorganic species in atmospheric aerosols during wintertime over urban and high-altitude sites in North India. *J. Geophys. Res.: Atmosphere* 112, D21307.
- Samburova, V., Connolly, J., Gyawali, M., Yatawelli, R.L.N., Watts, A.C., Chakrabarty, R.K., Zielinska, B., Moosmüller, H., Khlystov, A., 2016. Polycyclic aromatic hydrocarbons in biomass-burning emissions and their contribution to light absorption and aerosol toxicity. *Sci. Total Environ.* 568, 391–401.
- Shen, Z., Zhang, Q., Cao, J., Zhang, L., Lei, Y., Huang, Y., Huang, R.J., Gao, J., Zhao, Z., Zhu, C., Yin, X., Zheng, C., Xu, H., Liu, S., 2017. Optical properties and possible sources of brown carbon in PM<sub>2.5</sub> over Xi'an, China. *Atmos. Environ.* 150, 322–330.
- Simoneit, B.R.T., Schauer, J.J., Nolte, C.G., Oros, D.R., Elias, V.O., Fraser, M.P., Rogge, W.F., Cass, G.R., 1999. Levoglucosan, a tracer for cellulose in biomass burning and atmospheric particles. *Atmos. Environ.* 33, 173–182.
- Srinivas, B., Rastogi, N., Sarin, M.M., Singh, A., Singh, D., 2016. Mass absorption efficiency of light absorbing organic aerosols from source region of paddy-residue burning emissions in the Indo-Gangetic Plain. *Atmos. Environ.* 125, 360–370 Part B.
- Srinivas, B., Sarin, M.M., 2014. Brown carbon in atmospheric outflow from the Indo-Gangetic Plain: mass absorption efficiency and temporal variability. *Atmos. Environ.* 89, 835–843.
- Sun, H., Biedermann, L., Bond, T.C., 2007. Color of brown carbon: a model for ultraviolet and visible light absorption by organic carbon aerosol. *Geophys. Res. Lett.* 34.
- Tian, J., Wang, Q., Ni, H., Wang, M., Zhou, Y., Han, Y., Shen, Z., Pongpiachan, S., Zhang, N., Zhao, Z., Zhang, Q., Zhang, Y., Long, X., Cao, J., 2019. Emission characteristics of primary Brown carbon absorption from biomass and coal burning: development of an optical emission inventory for China. *J. Geophys. Res.: Atmosphere* 124, 1879–1893.
- Turpin, B.J., Huntzicker, J.J., 1995. Identification of secondary organic aerosol episodes and quantitation of primary and secondary organic aerosol concentrations during SCAQS. *Atmos. Environ.* 29, 3527–3544.
- Virkkula, A., Ahlquist, N.C., Covert, D.S., Arnott, W.P., Sheridan, P.J., Quinn, P.K., Coffman, D.J., 2005. Modification, calibration and a field test of an instrument for measuring light absorption by particles. *Aerosol Sci. Technol.* 39, 68–83.
- Watson, J.G., Tropp, R.J., Kohl, S.D., Wang, X., Chow, J.C., 2017. Filter processing and gravimetric analysis for suspended particulate matter samples. *Aerosol Sci. Eng.* 1, 93–105.
- Wu, G.-M., Cong, Z.-Y., Kang, S.-C., Kawamura, K., Fu, P.-Q., Zhang, Y.-L., Wan, X., Gao, S.-P., Liu, B., 2016. Brown carbon in the cryosphere: current knowledge and perspective. *Adv. Clim. Change Res.* 7, 82–89.
- Wu, G., Ram, K., Fu, P., Wang, W., Zhang, Y., Liu, X., Stone, E.A., Pradhan, B.B., Dangol, P.M., Panday, A.K., Wan, X., Bai, Z., Kang, S., Zhang, Q., Cong, Z., 2019. Water-soluble Brown carbon in atmospheric aerosols from godavari (Nepal), a regional representative of south Asia. *Environ. Sci. Technol.* 53, 3471–3479.
- Xia, X., Zong, X., Cong, Z., Chen, H., Kang, S., Wang, P., 2011. Baseline continental aerosol over the central Tibetan plateau and a case study of aerosol transport from South Asia. *Atmos. Environ.* 45, 7370–7378.
- Xu, H., Cao, J., Chow, J.C., Huang, R.J., Shen, Z., Chen, L.W.A., Ho, K.F., Watson, J.G., 2016. Inter-annual variability of wintertime PM<sub>2.5</sub> chemical composition in Xi'an, China: Evidences of changing source emissions. *Sci. Total Environ.* 545–546, 546–555.
- Yang, M., Howell, S.G., Zhuang, J., Huebert, B.J., 2009. Attribution of aerosol light absorption to black carbon, brown carbon, and dust in China – interpretations of atmospheric measurements during EAST-AIRE. *Atmos. Chem. Phys.* 9, 2035–2050.
- Yang, S., Xu, B., Cao, J., Zender, C.S., Wang, M., 2015. Climate effect of black carbon aerosol in a Tibetan Plateau glacier. *Atmos. Environ.* 111, 71–78.
- Zhao, Z., Cao, J., Shen, Z., Xu, B., Zhu, C., Chen, L.W.A., Su, X., Liu, S., Han, Y., Wang, G., 2013. Aerosol particles at a high-altitude site on the Southeast Tibetan Plateau, China: implications for pollution transport from South Asia. *J. Geophys. Res.: Atmosphere* 118, 11360–11375.
- Zhao, Z., Wang, Q., Xu, B., Shen, Z., Huang, R., Zhu, C., Su, X., Zhao, S., Long, X., Liu, S., Cao, J., 2017. Black carbon aerosol and its radiative impact at a high-altitude remote site on the southeastern Tibet Plateau. *J. Geophys. Res.: Atmosphere* 122, 5515–5530.
- Zhu, C.-S., Cao, J.-J., Hu, T.-F., Shen, Z.-X., Tie, X.-X., Huang, H., Wang, Q.-Y., Huang, R.-J., Zhao, Z.-Z., Močnik, G., Hansen, A.D.A., 2017. Spectral dependence of aerosol light absorption at an urban and a remote site over the Tibetan Plateau. *Sci. Total Environ.* 590–591, 14–21.